Computational Particle Mechanics
https://doi.org/10.1007/s40571-019-00300-w

Numerical analysis of flyer plate experiments in granite via the combined finite–discrete element method

Viet Chau[1] · Esteban Rougier[1] · Zhou Lei[1] · Earl E. Knight[1] · Ke Gao[1] · Abigail Hunter[1] · Gowri Srinivasan[1] · Hari Viswanathan[1]

Received: 16 May 2019 / Revised: 3 November 2019 / Accepted: 7 November 2019

Abstract
In this study, the combined finite–discrete element method (FDEM), which merges the finite element-based analysis of continua with discrete element-based transient dynamics, contact detection, and contact interaction solutions, is used to simulate the response of a flyer plate impact experiment in a Westerly granite sample that contains a randomized set of cracks. FDEM has demonstrated to be a strongly improved physical model as it can accurately reproduce the velocity interferometer system for any reflector plot and capture the spall region and spall strength obtained from flyer plate experiments in granite. The number and the distributions of preexisting fractures have also been studied to get better understanding of the effect of structural cracks on the mechanical behavior and the failure path of Westerly granite under high strain rate impact. These FDEM capabilities, in the context of rock mechanics, are very important for two main reasons. First, the FDEM can be further applied to many complex large-scale problems such as planetary impact, rock blasting, seismic wave propagation, characterization of material failure around explosive crater formations, and detection of hydrocarbon flow in petroleum industry. Second, it can be used to validate high strain rate impact experiments and essentially, via virtual experimentation, replace these high-cost experiments by very cost- and time-effective simulations.

Keywords Combined finite–discrete element method (FDEM) · Brittle material · High strain rate · Flyer plate, granite

1 Introduction

The shock-induced response of geological materials has been a focus of research efforts for the last several decades due to its importance for many fields and applications including impact and explosive crater formations in planetary science, response of geomaterials to blast/explosive loading for underground explosion detection and discrimination, and rock fragmentation processes which are very relevant to the energy industry due to the use of innovative high strain rate fracking techniques. In these applications, strain rates of the order of 10^5 s^{-1} and higher are common, and therefore, loading processes are usually adiabatic. In a recent article by Yuan and Prakash, they study these issues by conducting novel plate impact experiments designed specifically to investigate inelasticity and shock-induced response in Westerly granite rock samples [1]. They use multi-beam VALYN velocity interferometer for any reflector (VISAR) to measure the free surface particle velocity in order to calculate the spall strength following the shock-induced compression in Westerly granite samples [2]. However, in many cases, such as planetary science applications, experimental evidence, or data often do not exist for these systems. Thus, reliable numerical models are critical for the prediction of material strength and failure behavior necessary for studying, optimizing, and developing critical processes for these applications.

With the rapid development of high-performance computing capabilities and new numerical approaches, various modeling tools have been employed to study the behavior of brittle materials under high strain rate impact loading conditions [3]. Among the 2D numerical studies, the work of Liu and Wang can be mentioned [4, 5]. Both of these studies utilized in-house numerical tools that do not account for inelastic strains in the rock to study rock fragmentation following indention [4]. Another example of 2D numerical modeling is the work by Saksala where a viscoplastic consistency model and an isotropic damage description are coupled to take both

✉ Viet Chau
vchau@lanl.gov

Esteban Rougier
erougier@lanl.gov

[1] Los Alamos National Laboratory, Los Alamos, NM, USA

Published online: 20 November 2019

the compressive and the tensile responses of the rock into account [6]. Among the studies using discontinuous mechanics approach, Thuro et al. [7] used a Particle Flow Code (PFC2D) to investigate the crack pattern. A continuum approach was used by Forquin and Hild to study the dynamic fragmentation as a result of impact loading in a wide range of brittle materials (e.g., concrete, ceramics, silicate glass, and rock) [8]. However, being a continuum-based model, certain constraints (such as re-meshing problem and element deletion constraint due to excessive element distortion) arrive after the material breaks into fragments that are ejected as a consequence of the high strain rate impact load.

From a computational mechanics point of view, the simulation of high strain rate processes is challenging because upon failure a brittle material, such as granite, undergoes significant failure and fragmentation, with the resulting particles experiencing significant displacement and rotation during the process [9]. Numerical models based purely on a continuum assumption, such as the finite element method, have been used extensively for this purpose; however, the limitations connected with the assumption of a continuum medium become increasingly constraining when trying to simulate the material behavior in the post-failure regime. Because of these reasons, a numerical tool that has the capability of handling continua and discontinua simultaneously would be useful [10]. Fortunately, a recently developed numerical method—the combined finite–discrete element method (FDEM) [11–14], which merges finite element-based analysis of continua with discrete element-based transient dynamics, contact detection and contact interaction solutions of discontinua, provides a natural solution to modeling high-velocity impact problem in brittle material.

In this work, the FDEM is used to investigate the behavior of brittle materials under high strain rate loading. In the following sections, we first provide the reader with a brief introduction to the theories of FDEM. Then, we illustrate the setup of the numerical model. The tests were numerically modeled, and the results were compared with the experimental data in order to validate the model. Furthermore, in the present study, the effect of the presence of preexisting cracks (with different lengths and orientations) in the material is analyzed in detail and the simulations are directly compared with the experimental observations. The simulation capabilities of FDEM for modeling flyer plate experiments are explored for the first time in the research community.

2 The combined finite–discrete element method (FDEM)

The FDEM was originally developed by Munjiza in the early 1990s to simulate the transition behavior of material from continuum to discontinuum [14]. The essence of this method is to merge the algorithmic advantages of the DEM with those of the finite element method (FEM) [15]. The main theory of the FDEM can be broadly broken down into the following parts: governing equations, finite strain-based formulation for deformation description, contact detection, and contact interaction algorithms [16–18]. In this work, an in-house implementation of FDEM called HOSS (Hybrid Optimization Software Suite) was used to simulate the flyer plate experiment [19–21].

2.1 Governing equations

The general governing equation of the FDEM is [11]

$$\mathbf{M}\ddot{\mathbf{x}} + \mathbf{C}\dot{\mathbf{x}} = \mathbf{f}, \tag{1}$$

where $\mathbf{M}$ is the lumped mass matrix, $\mathbf{C}$ is the damping matrix, $\mathbf{x}$ is the displacement vector, and $\mathbf{f}$ is the equivalent force vector acting on each node which includes all forces existing in the system such as the forces due to material deformation and contact forces between solid elements. An explicit time integration scheme based on a central difference method is employed to solve Eq. (1) with respect to time in order to obtain the transient evolution of the system.

2.2 Finite strain-based formulation

In FDEM, each discrete element consists of a subset of finite elements that are allowed to deform according to the applied loads. Deformation of the finite elements is described by a multiplicative decomposition-based formulation [13]. This framework allows for a uniform solution for both isotropic and general anisotropic materials for capturing detailed material deformation [16]. Moreover, volumetric locking due to the lower-order finite element implementations can be eliminated by using a selective stress integration scheme.

2.3 Contact detection

The contact detection between discrete elements is conducted using the MRCK (Munjiza–Rougier–Carney–Knight) algorithm which is based on the decomposition of the simulation space into identical square (two-dimensional) or cubical (three-dimensional) search cells [12, 22]. Consider that for any two given particles or elements, one called the contactor and the other one the target, both are mapped onto search cells according to their current position. A more in detail description of the contact detection strategy is beyond the scope of this paper; however, the interested reader is referred to [12] for more information. The goal of the contact search process is to determine whether the contactor and the target share at least one cell. After processing the contact detection, a list that contains all the pairs of elements potentially in contact is established and sent for contact interaction

process [15]. The MRCK contact detection algorithm has proven to be highly efficient resulting in a theoretical CPU time proportional to the total number of elements present in the system, and it is applicable to systems consisting of many bodies of different shapes and sizes [22].

2.4 Damage modeling

In HOSS, cracks form along the boundaries of the finite elements. In order to capture fine mechanisms, such as crack nucleation, propagation, branching, and reorientation, the crack networks must be finely resolved spatially, with dozens to hundreds of finite elements along the length of each crack [23].

The problem of interest for this work (described in more detail in the next section) is a 2D sample under high-velocity impact loading. For the purpose of fracture modeling, HOSS considers two primary modes of failure in 2D: Mode I, which is opening due to tensile load, and Mode II, which is crack growth due to shear loading conditions [11, 12, 14, 17]. FDEM in HOSS can also allow for mixed mode crack in a consistent formulation. This feature is not always implemented in other numerical methods. Since the problem of interest will be mainly dominated by Mode I crack growth, we focus this discussion on the key details as to how HOSS accounts for Mode I crack growth. However, it must be pointed out that the Mode II crack growth is handled in a similar way to the Mode I case, except that different sets of parameters are applied. It is worth noting that, although globally Mode I failure dominates this problem, both shear and opening can occur at a local mesh element scale. In addition to the cohesion in shear, FDEM can also allow for modeling friction (either constant friction or elaborated friction law) even after the cohesion is fully broken.

Between the interface of any two finite elements, there lie a user-specified number of cohesive points (four are used in all simulations presented and discussed here), which are modeled as nonlinear springs, as shown in Fig. 1. As the two elements shown in the figure undergo tensile load and are pulled apart, the springs within the interface are strained resulting in a small space opening between the elements. Similarly, for shear, or Mode II, deformation, there will be four cohesive points that describe the shear stresses generated when one element slides relative to its neighbor. A typical behavior of the springs as a function of the opening (displacement) created between the edges of two finite elements is shown in Fig. 1.

These cohesive points between elements are responsible for representing the material strength response both in tension and in shear. The maximum stress that the springs can withstand in tension is equal to the tensile strength of the material ($\sigma_n^{\max}$), while the maximum shear stress that the analogous springs can carry is equal

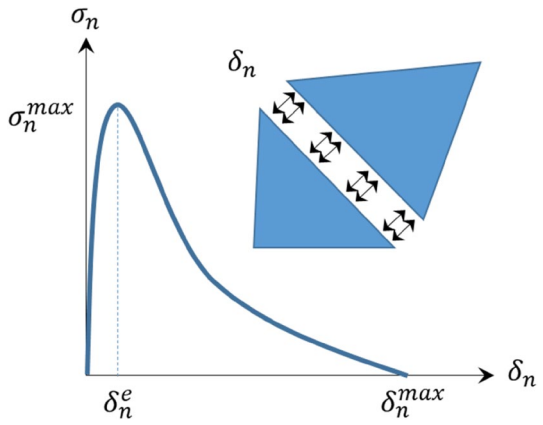

Fig. 1 Schematic representation of how damage is modeled in HOSS. $\sigma_n^{\max}$ is the tensile strength of the material, δ_n is the normal opening (represented in terms of displacements, not strains), δ_n^e is the elastic threshold for the cohesive spring, while $\delta_n^{\max}$ is the maximum allowable opening

to the shear strength of the material. In the first part of the curve ($0 < \delta_n \leq \delta_n^e$), the springs follow nonlinear elastic behavior where no irreversible damage is accrued. The springs connecting any two finite elements are very stiff in their nonlinear elastic response, i.e., $\delta_n^e \ll \delta_n^{\max}$ (the stiffness is, at least, two orders of magnitude larger than the Young's modulus of the material) in order to reproduce the response of a continuum medium. If the interface between the elements continues to be strained past this elastic limit $\left(\delta_n^e < \delta_n \leq \delta_n^{\max}\right)$, the springs enter a strain-softening regime which represents the material developing irreversible damage and therefore degrading its strength response. Once $\delta_n > \delta_n^{\max}$, the spring is considered to be broken and no longer supports any load. It is worth noting that the area below the softening portion of the curve, indicated in Fig. 1, represents the specific energy (measured in J/m^2) density dissipated during the fracture process. The specific fracture energy value is defined by the area under the cohesion curve, which is dissipated due to the fracturing process. The fracture energy is pre-defined in the FDEM framework. Figure 1 only presents a schematic representation of this curve. The actual shape of the curve is found through fitting to the experimental results that describe softening in geomaterials.

3 Model setup

In the recent study by Yuan and Prakash, plate impact experiments are employed to better understand the stress threshold for inelasticity in Westerly granite samples. The experiments are designed to obtain the Hugoniot elastic limit (HEL) as well as spall strength following the shock-induced compression in the samples. The plate impact experiments

are conducted using an 82.5-mm bore single-stage gas-gun facility. Figure 2 shows the schematic of the plate impact experimental configuration. The rear end of the projectile has a sealing O-ring and a Teflon key that slides keyway inside the gun barrel to prevent any rotation of the projectile. In our simulations, for simplicity, two-dimensional plane strain conditions are assumed due to the O-ring constraint that produces zero strain in the radial direction of the target plate. In order to mimic the Teflon key effect on the target plate, roller supports are placed on the left and right side of the target plate. The aluminum flyer impacts the thick granite target plate with an initial velocity v_0, which is modeled accordingly with the applied velocity on the flyer plate shown in Fig. 2. A polymethyl methacrylate (PMMA) window plate is placed behind the granite target plate to provide a reflective surface to enable particle velocity measurements by using a laser interferometer. The multi-beam VALYN VISAR is used as the interferometer system to measure the free surface particle velocity history at the rear surface of the target plate [1]. A sensor is placed in our FDEM model to record the particle velocity on the back of granite sample.

The problem of interest is shown schematically in Fig. 3. This figure illustrates the geometry of the FDEM model, which is based on the plate impact experiment. The model consists of three plates: aluminum flyer plate, granite target plate, and PMMA momentum trap. Within the sample, there are a number of preexisting cracks each with initial lengths determined by a power law distribution and randomly distributed orientations [24]. The probability density function (pdf) used for pre-seeding these cracks is as follows:

$$f(x) = \left[l_{\min}^{g} + x\left(l_{\max}^{g} - l_{\min}^{g}\right)\right]^{\frac{1}{g}} \tag{2}$$

In this case, the selected minimum crack length, $l_{\min}$, is 0.5 mm, while the selected maximum crack length, $l_{\max}$, is 3.5 mm, and the exponent of the power law, g, is 3.0.

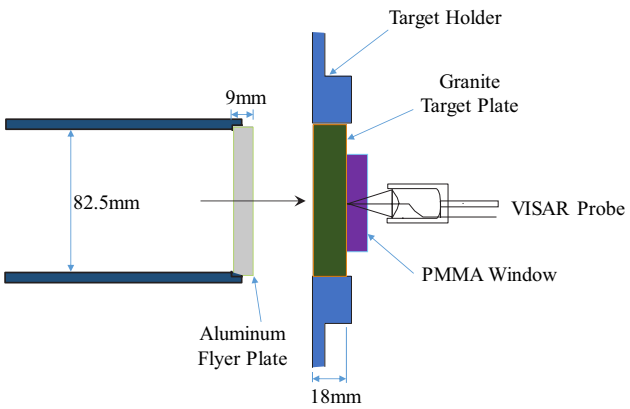

Fig. 2 Schematic of the flyer plate experiment (modified from [1])

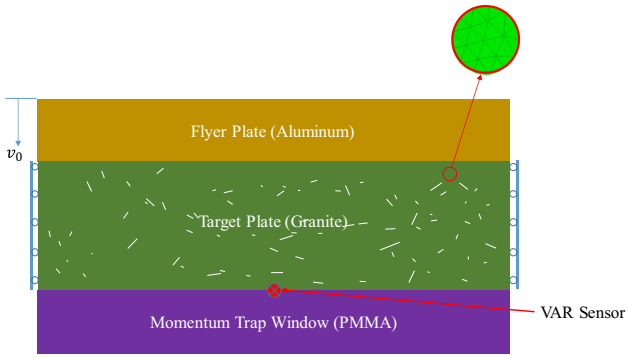

Fig. 3 Schematic of the FDEM setup for a flyer plate simulation

Preexisting cracks are defined as initially zero cohesion between the elements, while initial cohesion $\sigma_n^{\max}$ is uniformly applied on the other boundary of elements. A simple FDEM realization of the flyer plate setup is presented in Fig. 3 where each plate is represented by a discrete element, which allows for the tracking of their motion and their interactions with neighboring objects, and each discrete element is further discretized into finite elements in order to capture its deformation and stress evolution when subjected to external forces.

The FDEM material parameters for Westerly granite have been determined based on the previously reported experimental results. The granite target plate has a Young's modulus of 59.3 GPa and Poisson's ratio of 0.28, while the Young's modulus and Poisson's ratio of the aluminum flyer plate are 80.7 GPa and 0.3, respectively. The tensile and shear strength of the target plate are 12.5 MPa and 56.9 MPa, respectively. The maximum normal and tangential displacements are 0.018 mm (Table 1). The Young's modulus and Poisson's ratio of the PMMA are estimated to be 5.0 GPa and 0.36, respectively. These materials are assumed to be elastically isotropic. The elastic properties are obtained from the previously mentioned laboratory experiment.

Within the FDEM framework, contact interaction is resolved using the penalty method approach [12]. When contact couples are identified, a penalty function-based contact interaction algorithm is used to calculate the contact forces between contacting elements. In the penalty function method, a small penetration or overlap is allowed

Table 1 Granite material properties

Young's modulus	59.3 GPa
Poisson's ratio	0.28
Tensile strength	12.5 MPa
Shear strength	56.9 MPa
Maximum normal displacement	0.018 mm
Maximum tangential displacement	0.018 mm

between elements in contact, which then determines the normal contact force (magnitude and direction) acting on the contacting elements. This approach employs a penalty parameter in order to calculate the contact force. To achieve perfect contact without overlapping, this penalty parameter should be infinity. Since this is not numerically possible, a large but finite penalty parameter is employed. A recent study shows that in general a penalty parameter that is about 1–2 orders of magnitude larger than the Young's modulus of the material will ensure the correctness of the results [25]. By compromising between achieving the correct elastic response between contact elements and maximizing the time step size in order to reduce the overall computational expense, a penalty parameter one hundred times larger than the particles' Young's modulus, i.e., 5930 GPa, is used. Detailed material and calculation parameters are tabulated in Table 2.

There were about 193,000 constant strain triangle (CST) elements used in the model. The CST element size was 0.2 mm. The simulations were run for 60,000 time steps, with a time step of 3×10^{-5} μs. The total time in each simulation is 18 μs. The results from HOSS were output every 400 time steps, providing 150 output files of data per simulation. Each HOSS simulation took about 1 h of computation time on 140 processors in parallel.

4 Simulation results

4.1 Model evolution and validation with experiment

Initially, the purely hyper-elastic finite element model (i.e., no fracturing of the material is allowed) is employed to simulate the flyer plate experiment. As shown in Fig. 4, the hyper-elastic model can predict quite well the maximum velocity in the VISAR plot. However, instead of capturing the pullback signal observed in the experiment, the model predicts a sharp drop in the velocity, which returns to zero, after the peak. This inconsistent result for the purely elastic case is obtained because the material is not allowed to break/fracture. Therefore, the transition from continua to discontinua capability in the combined FDEM is the key factor to capture the physics at high-rate impact for brittle materials.

As shown in Fig. 5, the simulation for the impact velocity of 91.5 m/s can capture the VISAR plot very well when the FDEM model is used. First, the longitudinal wave propagation takes about 3 μs to travel from the top to the bottom of the target plate. Once the wave reaches the bottom, the velocity at free surface increases significantly to the maximum of about 82 m/s. The velocity keeps almost constant until the shock front rebounds from the PMMA window and travels back to interact with the release wave, creating a tensile stress state and corresponding fracture or spall region. Due to the high density of fractures generated in the spall region, the target plate is separated into two parts. Since there is a PMMA plate placed behind the granite plate, the free surface velocity at the bottom of the granite plate drops drastically at 6 μs and fluctuates at around 50 m/s. If the PMMA plate is removed, after the peak, the free surface velocity drops to approximately the initial impact velocity of 91.5 m/s (Fig. 6). This agrees with the argument mentioned in the experimental paper by Yuan and Prakash [1] where they claimed that in the spall experiments without the PMMA window plate, the free surface velocity after peak is expected to be equal to the impact velocity.

From our simulation results, the spall strength, σ_{spall}, can be calculated from the estimated particle velocities $V_{\max}$ and $V_{\min}$ by using the following equations:

$$\begin{aligned} \sigma_{\text{spall}} &= \frac{V_B - V_A}{2}\left(\rho C_L\right)_{\text{granite}} \\ V_B &= \frac{\left(\rho C_L\right)_{\text{granite}} - \left(\rho C_L\right)_{\text{PMMA}}}{\left(\rho C_L\right)_{\text{granite}}} V_{\max} \\ V_A &= \frac{\left(\rho C_L\right)_{\text{granite}} + \left(\rho C_L\right)_{\text{PMMA}}}{\left(\rho C_L\right)_{\text{granite}}} V_{\min} \end{aligned} \tag{3}$$

Table 2 Material and numerical simulation parameters

Impact velocity (m/s)	Flyer plate material	Flyer thickness (mm)	Target (granite) thickness (mm)	Impact stress (GPa)
91.5	Aluminum	8.85	19.05	0.7
156.5	Aluminum	9.12	18.90	1.2
249.1	Aluminum	8.95	18.70	1.8
364.5	Aluminum	8.95	19.01	2.9

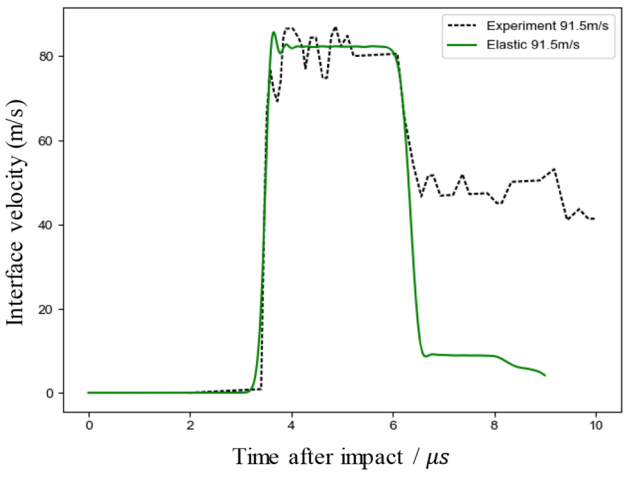

Fig. 4 Particle velocity versus time plot. Comparison between purely elastic simulation versus experiment, at impact velocity of 91.5 m/s

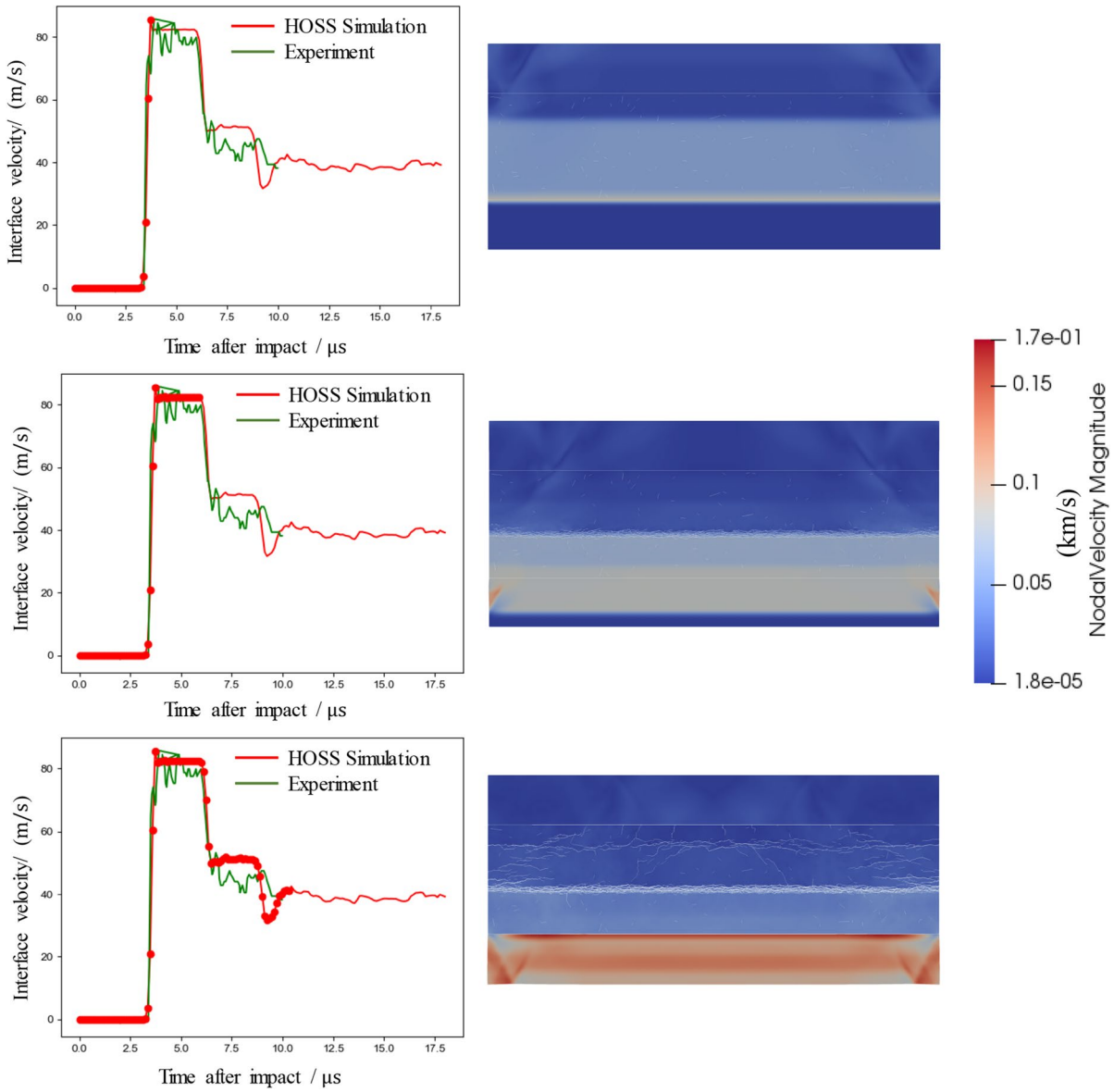

Fig. 5 Particle velocity versus time (left) and corresponding nodal velocity profile (right) for an impact velocity of 91.5 m/s at different times: 3 μs, 9 μs, and 18 μs

where $(\rho C_L)_{\text{granite}}$ and $(\rho C_L)_{\text{PMMA}}$ represent the longitudinal impedance of granite and PMMA, respectively.

As shown in Table 3, the spall strength of the Westerly granite at different impact stresses (or impact velocities) is calculated from the simulation results and is approximately 48 MPa. It is found that the spall strengths estimated from the experiments are in very good agreement with those from simulation, and it is nearly independent of the applied compression stress levels in the experiments. In overall, the simulated results slightly overpredict the experimental values due to the fact that the material model used for calculating the stresses is elastic and therefore does not consider plastic processes (at the material point level inside the finite elements) that may take place in this type of experiment.

Figure 7 shows the free surface velocity from experiments and simulations at different impact velocities. As can be seen clearly, the FDEM model can match the overall trend of the experiments very well, especially for the lower velocity impacts. The granite material is expected to remain elastic at the low impact velocities of 91.5 m/s, 156.5 m/s, 249.1 m/s, and 364.5 m/s, but show significant inelasticity at the higher impact velocities, i.e., 561.3 m/s, 491.5 m/s, and 489.4 m/s.

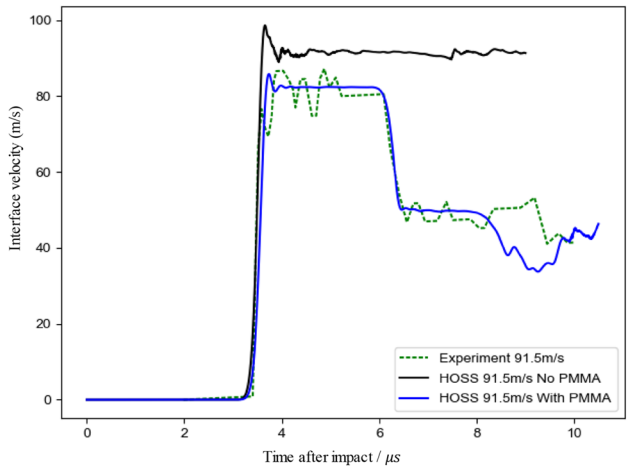

Fig. 6 Particle velocity plot demonstrating the effect of the presence of a PMMA window

Table 3 Spall strength calculated from simulation and experiment

	Experiment (MPa)	Simulation (MPa)	% Difference
Shot 1: $V=91.5$ m/s	41	43.5	6.09
Shot 2: $V=156$ m/s	46	46.67	1.45
Shot 3: $V=249.1$ m/s	45	48.45	7.67
Shot 4: $V=356.1$ m/s	47	50.15	6.7

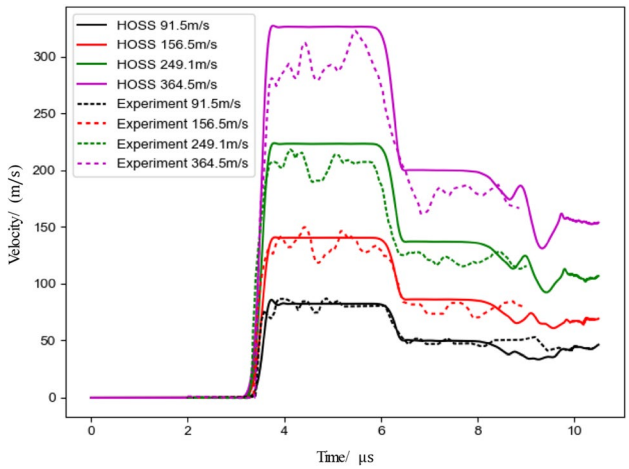

Fig. 7 Particle velocity versus time plot. Comparison between simulations versus experiments, at impact velocities of 91.5 m/s, 156.5 m/s, 249.1 m/s, and 364.5 m/s

Thus, in order to capture the higher strain rate experiments, we must include the plasticity model in the finite element part of the FDEM, which will be discussed in the subsequent paper.

Figures 8 and 9 show the nodal velocities and the crack propagation in the granite plate (denoted by the white lines) under different impact velocities. As can be observed clearly, the higher impact velocities will generate more fractures in comparison with the lower ones. However, the spall region locations are independent to the loading rates. At different loading rates, the spall regions are always at about 7.6 mm above the bottom of the granite plate. If the flyer plate has the same density as the target plate, the spall region will happen right at the middle of the granite plate. Also, the gap of fractures can be observed around the middle of top-half across the spall region of target plate (Figs. 5 and 8). This might be due to the bending of top-half of target plate after forming spall region.

4.2 Effect of preexisting micro-cracks

The aim of this study is to investigate the effect of preexisting, or structural, cracks on dynamic fragmentation of granite. Because of the complex behavior of rock materials, the FDEM is employed relying upon an elasticity model with an isotropic damage model with softening law. The preexisting cracks are introduced in the model by considering sets of elements that are fully damaged under both tensile and shear loading condition. The results from the analysis with power law distribution crack lengths and uniformly distributed orientations are compared in terms of fracture pattern and the VISAR plot.

The preexisting cracks with different lengths and orientations are introduced in the numerical simulation. As can be clearly seen in Fig. 10, the number of preexisting cracks does not affect the VISAR plot significantly, except for the case of 2000 preexisting cracks. In this 2000-crack case, due to many damaged elements placed in the granite sample, the longitudinal wave slightly falls behind, which creates a relatively small time lag at the beginning of the VISAR plot (Fig. 10). However, it is shown in Figs. 11 and 12 that the fracture patterns change noticeably from the case of no cracks to the 2000-crack case. Several simulations with 100 preexisting cracks but different initial crack orientations and locations were completed to study the effect of the

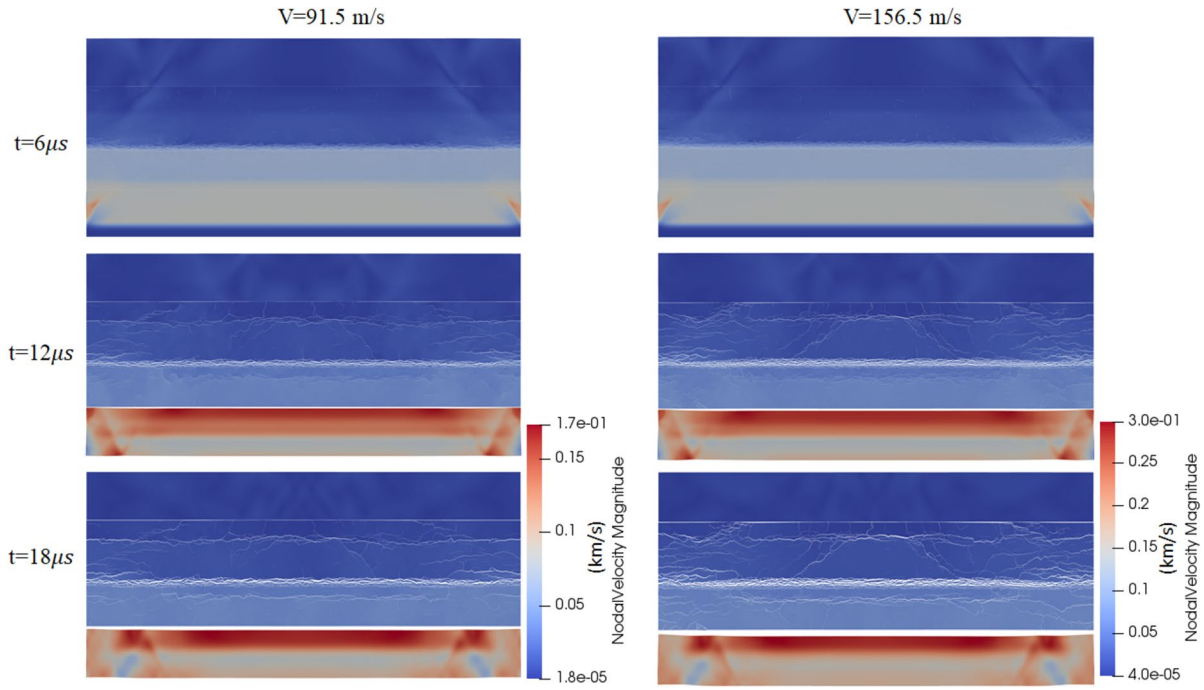

Fig. 8 Nodal velocity profile for different impact velocities: 91.5 m/s versus 156.5 m/s

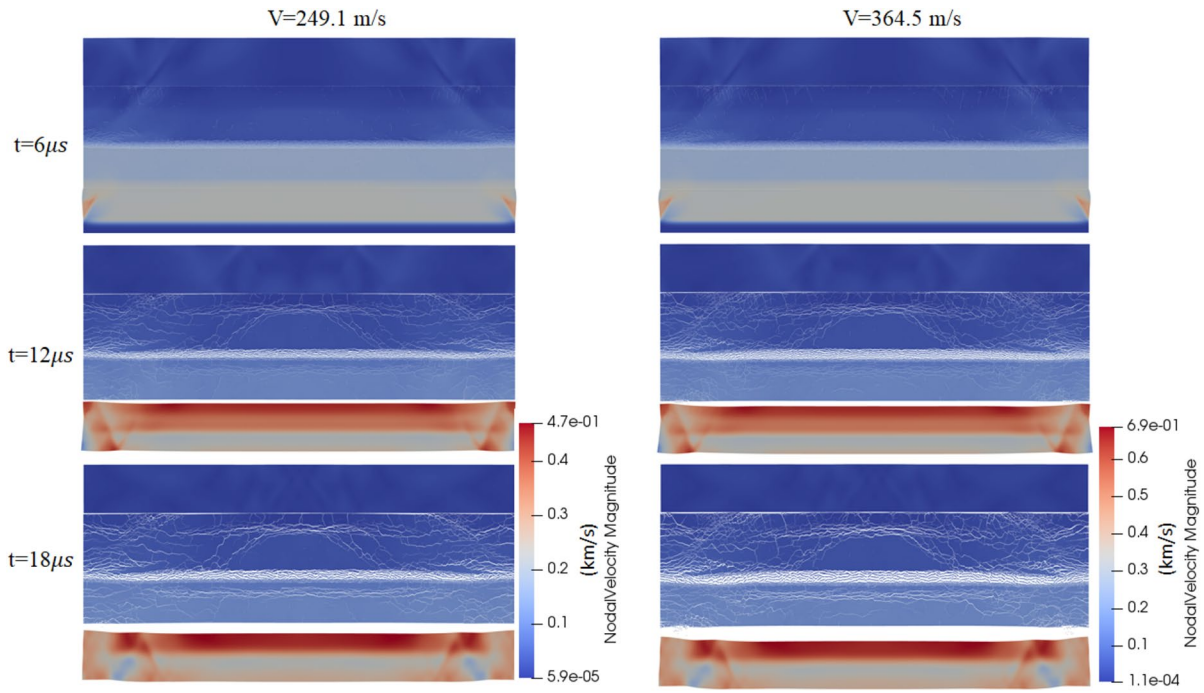

Fig. 9 Nodal velocity profile for different impact velocities: 249.1 m/s versus 364.5 m/s

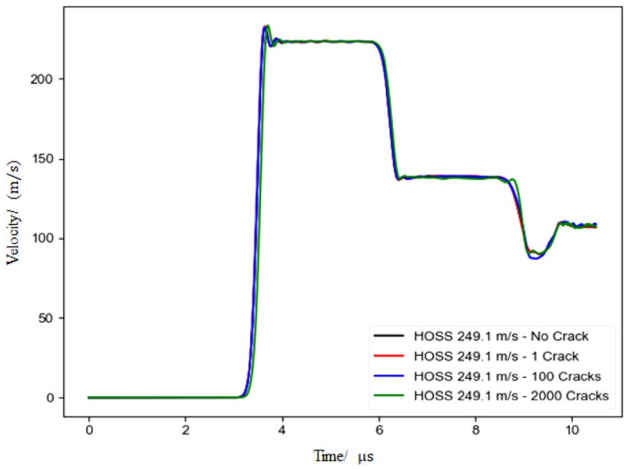

Fig. 10 Particle velocity plot demonstrating the effect of the presence of preexisting cracks in the simulation setup

prescribed distribution on the material response. However, there is no significant difference in the fracture pattern when changing the crack topology.

4.3 Effect of fracture energy

The aim of the work presented in this section is to investigate the effect of changes in the fracture energy of the material (as specified in the model, see Sect. 2.4) on the overall material response. The fracture energy is based on the approximation of the stress–strain curves for granite in direct tension and the tensile strength of the material. It can be clearly seen in Fig. 13 that for time <7 μs changes in the fracture energy do not have a large effect on the VISAR signal. After 7 μs, the main cracks start to fully develop at the spall region in the sample, and at that point the effect of fracture energies is observed even though it is still relatively minor. Even though the VISAR plots are slightly different for various fracture energy cases, the crack patterns change dramatically. Figures 14 and 15 show that the lower the fracture energy of the material is, the more fractures are generated in the granite plate. These results demonstrate that, for this type of problems, matching the VISAR does not provide enough constraints for calibrating a material model, as, for example, a histogram of the size or volume distribution of the fragments generated after the impact.

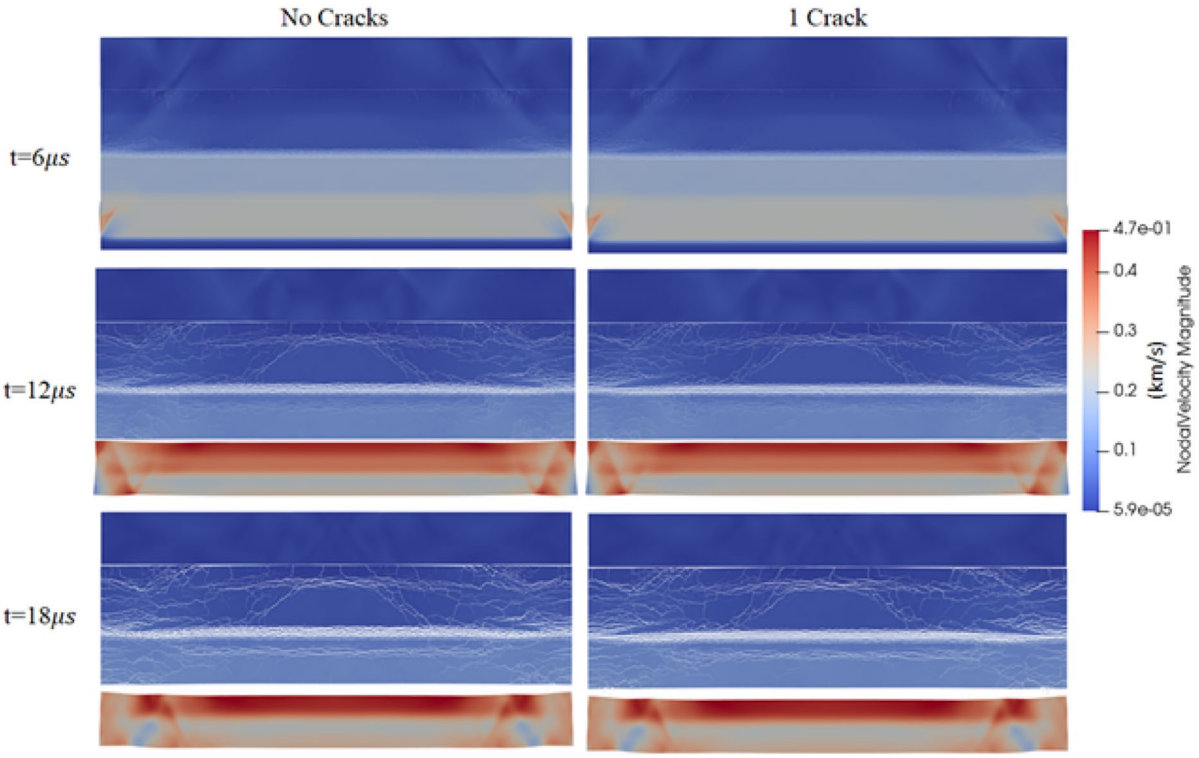

Fig. 11 Nodal velocity profile demonstrating for the effect of preexisting cracks: no crack versus 1 crack

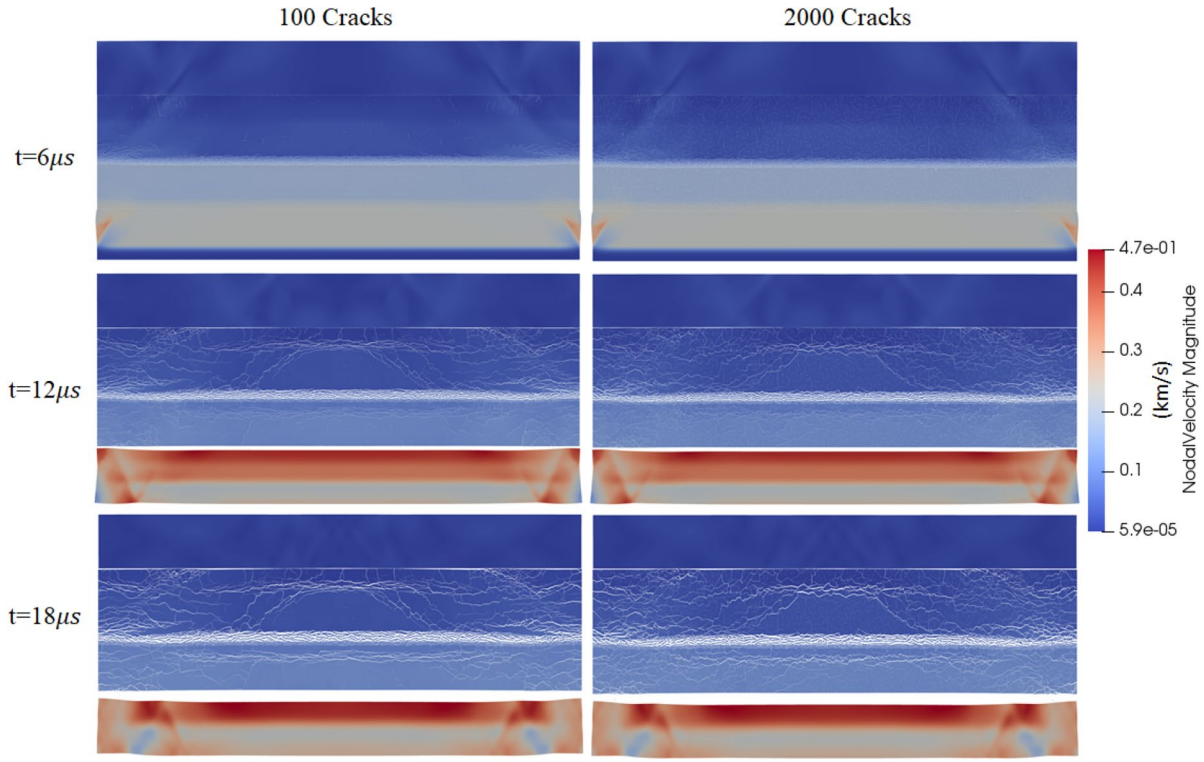

Fig. 12 Nodal velocity profile demonstrating for the effect of preexisting cracks: 100 versus 2000 cracks

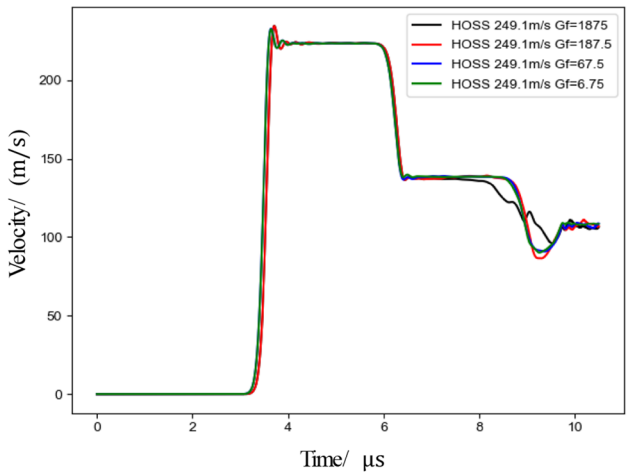

Fig. 13 Particle velocity plot demonstrating for the effect of changes in the fracture energy

5 Conclusions

In this work, an in-house implementation of the combined finite–discrete element method (HOSS) was employed to simulate flyer plate experiments on Westerly granite samples. The main conclusions obtained from this work are:

1. Simulated VISAR profiles show excellent matches to experimental VISAR profiles for an aluminum plate (flyer) impacting a granite plate. Multiple impact velocities were modeled and showed good matches for the spall strength calculations. The FDEM model does not need to calibrate many parameters like other pure continuum model or pure discrete models. All we need are the elastic material properties of granite, aluminum, and PMMA, such as Young modulus, density and Poisson ratio, and the strength properties, i.e., tensile and shear strengths and their associated specific fracture energies.
2. The number of preexisting cracks in the target plate does not affect the VISAR plot, but does considerably change the final fracture patterns in the granite sample. The number of preexisting cracks matters quite a lot in order to match the fracture patterns of the sample in the experiment.
3. The VISAR plot obtained from the simulations is practically indifferent to the changes on the specific fracture energies. However, that is not the case for the final fracture patterns, which show a strong dependence on the specific fracture energy used in the model.

Overall, it is interesting to find that the common metric used to quantify the overall material response for these types of experiments, the VISAR signal, can be well

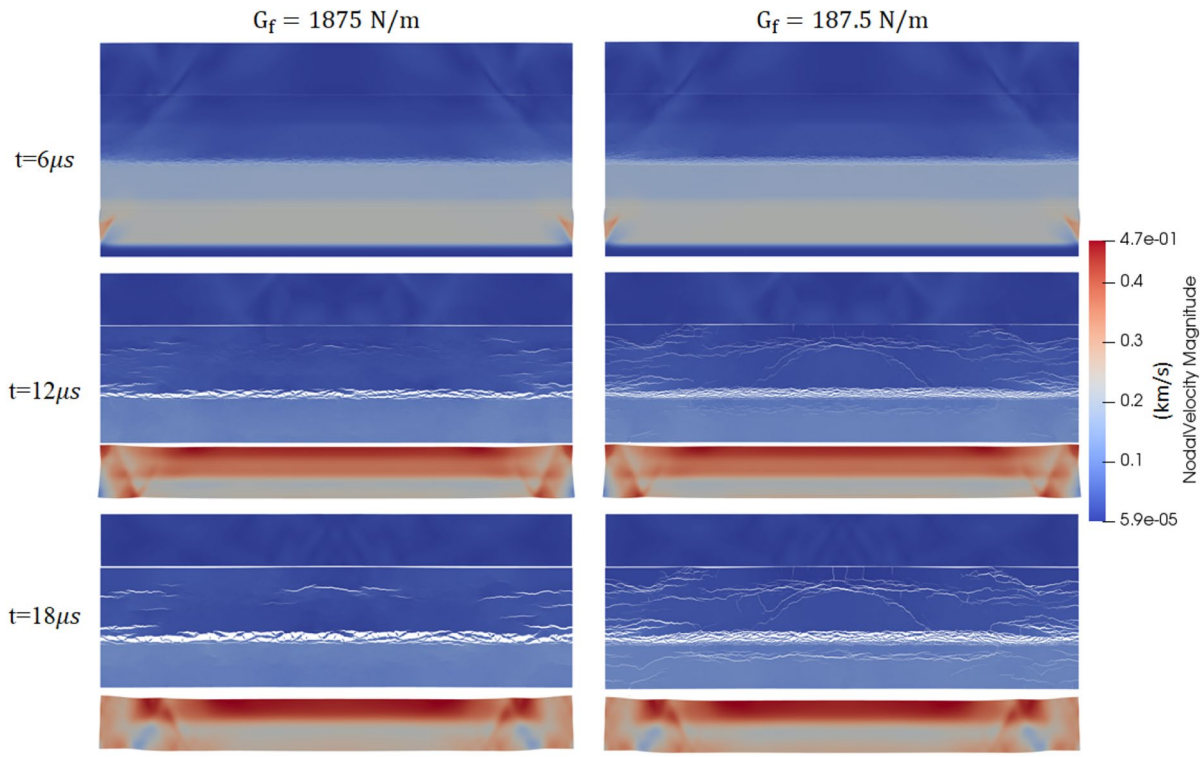

Fig. 14 Nodal velocity profile demonstrating for the effect of fracture energy

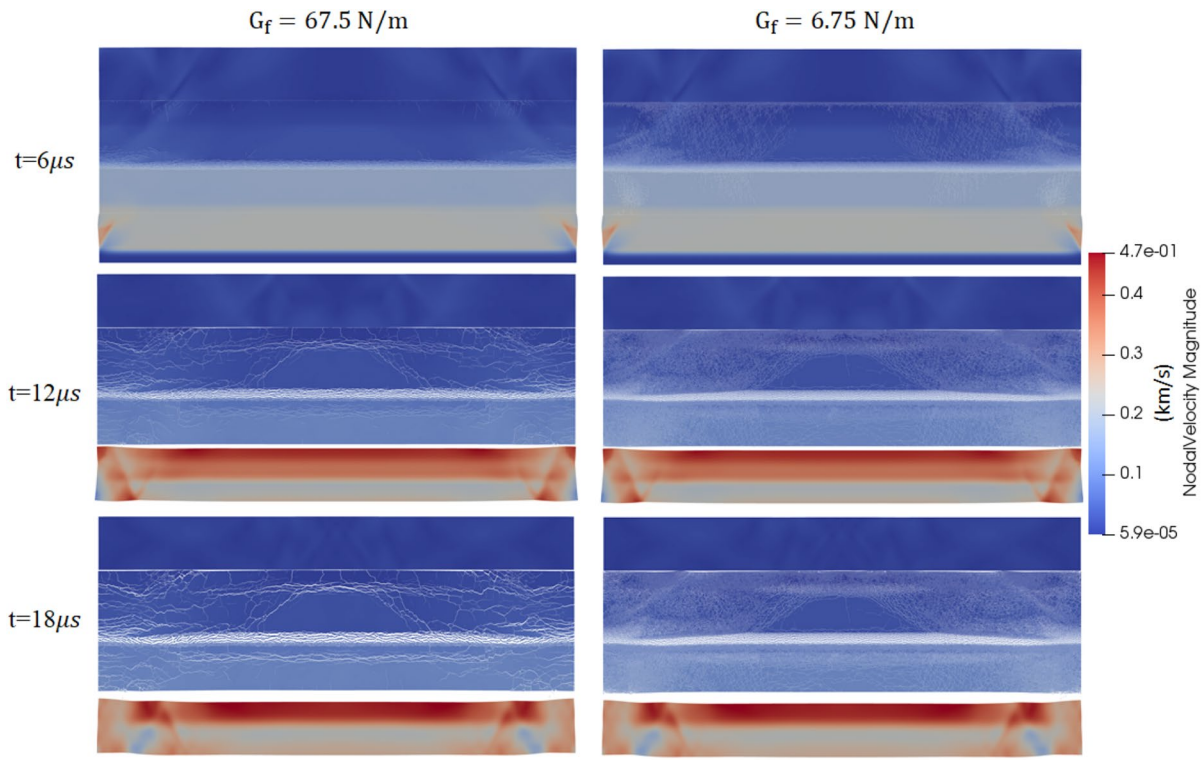

Fig. 15 Nodal velocity profile demonstrating for the effect of fracture energy

matched, while the final fracture patterns can vary so widely based on changes to the specific fracture energy and/or preexisting crack network. This motivates the need for models, such as the FDEM, which can explicitly capture the fracturing behavior of the material in addition to common metrics that can be measured experimentally. Such approaches can ensure that the fracturing process itself is accurately modeled.

Acknowledgements The Los Alamos National Laboratory LDRD Program (Project #20170103DR) supported this work. Technical support and computational resources from the Los Alamos National Laboratory Institutional Computing Program are highly appreciated. Our data are available by contacting the corresponding authors.

References

1. Yuan F, Prakash V (2013) Plate impact experiments to investigate shock-induced inelasticity in Westerly granite. Int J Rock Mech Min Sci 60:277–287
2. Prakash V (1995) A pressure-shear plate impact experiment for investigating transient friction. Exp Mech 35(4):329–336
3. Zhao H, Gary G (1995) A three dimensional analytical solution of the longitudinal wave propagation in an infinite linear viscoelastic cylindrical bar. Application to experimental techniques. J Mech Phys Solids 43(8):1335–1348
4. Liu H, Kou S, Lindqvist P-A, Tang C (2002) Numerical simulation of the rock fragmentation process induced by indenters. Int J Rock Mech Min Sci 39(4):491–505
5. Wang S, Sloan S, Liu H, Tang C (2011) Numerical simulation of the rock fragmentation process induced by two drill bits subjected to static and dynamic (impact) loading. Rock Mech Rock Eng 44(3):317–332
6. Saksala T (2010) Damage–viscoplastic consistency model with a parabolic cap for rocks with brittle and ductile behavior under low-velocity impact loading. Int J Numer Anal Methods Geomech 34(13):1362–1386
7. Thuro K, Schormair NJ (2008) Fracture propagation in anisotropic rock during drilling and cutting. Geomechanik und Tunnelbau 1(1):8–17
8. Forquin P, Hild F (2010) A probabilistic damage model of the dynamic fragmentation process in brittle materials. In: Advances in applied mechanics, vol 44. Elsevier, pp 1–72
9. Rougier E, Knight EE, Broome ST, Sussman AJ, Munjiza A (2014) Validation of a three-dimensional finite-discrete element method using experimental results of the split Hopkinson pressure bar test. Int J Rock Mech Min Sci 70:101–108
10. Shockey DA, Curran DR, Seaman L, Rosenberg JT, Petersen CF (1974) Fragmentation of rock under dynamic loads. In: International journal of rock mechanics and mining sciences and geomechanics abstracts, vol 8. Elsevier, pp 303–317
11. Munjiza AA (2004) The combined finite-discrete element method. Wiley, Hoboken
12. Munjiza AA, Knight EE, Rougier E (2011) Computational mechanics of discontinua. Wiley, Hoboken
13. Munjiza AA, Rougier E, Knight EE (2014) Large strain finite element method: a practical course. Wiley, Hoboken
14. Munjiza A (1992) Discrete elements in transient dynamics of fractured media. Swansea University, Swansea
15. Gao K, Euser BJ, Rougier E, Guyer RA, Lei Z, Knight EE, Carmeliet J, Johnson PA (2018) Modeling of stick-slip behavior in sheared granular fault gouge using the combined finite–discrete element method. J Geophys Res Solid Earth 123(7):5774–5792
16. Lei Z, Rougier E, Knight EE, Munjiza AA, Viswanathan H (2016) A generalized anisotropic deformation formulation for geomaterials. Comput Part Mech 3(2):215–228. https://doi.org/10.1007/s40571-015-0079-y
17. Munjiza A, Rougier E, John NWM (2006) MR linear contact detection algorithm. Int J Numer Methods Eng 66(1):46–71. https://doi.org/10.1002/nme.1538
18. Munjiza A, Andrews K (1998) NBS contact detection algorithm for bodies of similar size. Int J Numer Methods Eng 43(1):131–149
19. Knight E, Rougier E, Munjiza AJP, LA-UR-13-23409 (2013) LANL-CSM: Consortium proposal for the advancement of HOSS.05-09
20. Rougier E, Knight E, Munjiza AJP, LA-UR-13-23422 (2013) LANL-CSM: HOSS-MUNROU Technology Overview.05-10
21. Knight E, Rougier E, Lei Z (2015) Hybrid optimization software suite (HOSS)-educational version. In: Technical report LA-UR-15-27013. Los Alamos National Laboratory
22. Rougier E, Munjiza AA (2010) MRCK_3D contact detection algorithm. In: Paper presented at the proceedings of 5th international conference on discrete element methods. London
23. Knight E, Rougier E, Lei Z (2015) Hybrid optimization software suite (HOSS)—educational version. Technical Report LA-UR-15-27013, Los Alamos National Laboratory
24. Saadati M, Forquin P, Weddfelt K, Larsson PL, Hild F (2015) A numerical study of the influence from pre-existing cracks on granite rock fragmentation at percussive drilling. Int J Numer Anal Methods Geomech 39(5):558–570
25. Tatone BSA, Grasselli G (2015) A calibration procedure for two-dimensional laboratory-scale hybrid finite–discrete element simulations. Int J Rock Mech Min Sci 75(3):56–72. https://doi.org/10.1016/j.ijrmms.2015.01.011